Determination of in-plane shear properties of UD reference material

A comparison of the results obtained with different techniques

OB_TG2_R023 rev. 000

Confidential

OPTIMAT BLADES

TG 2

Arwen Smits
Danny Van Hemelrijck

UNIVERSITY OF PATRAS · Knowledge Centre WMC · ECN · TU Delft · DLR · VUB · ECN · KAПE CRES

Change record

Issue/revision	date	pages	summary of changes
Version 1	11-02-2005	31	na

Introduction

The aim of this report is to compare the in-plane shear properties of the OB UD material obtained with different test techniques. The shear modulus was obtained with three different test methods at the Free University of Brussels: the first method uses 30° off-axis specimens tested in tension, the second technique is the 'Resonalyser' technique developed at the department of Mechanics of Materials and Constructions and the third technique uses a torsion test bench. A short explanation of each technique will be given in the subsequent paragraphs. In the last paragraph a comparison between the obtained shear moduli will be made. The in-plane shear properties obtained at other institutes (UP and RISOE) will also be added for comparison.

1. Static tension tests on 30° off-axis specimens

1.1. Principle and set-up

The tests are performed on an INSTRON 4505 test machine with a capacity of 100kN in tension. The load is applied displacement controlled with a test speed of 0.25 mm/minute. The strains are measured in the loading direction, perpendicular to the loading direction and in the 45° direction at both sides of the specimens. The strain gauges used are from Tokyo Sokki Kenkyujo Co., Ltd. The strain gauge type is FRA-6. The gauge length is 6 mm and the gauge width 2.4 mm. The strain gauge types and gage factors are indicated in Table 1. The tests were loading-unloading-reloading static increasing tests performed for TG 3. The material tested was OB UD material existing of 4 layers, but cut with fibres at 30°.

	strain gauges		gage factor	
	left side	right side	left side	right side
GEV206_R0330_12	FRA-6	FRA-6	2.11	2.11
GEV206_R0330_13	FRA-6	FRA-6	2.11	2.11
GEV206_R0330_14	FRA-6	FRA-6	2.11	2.11
GEV206_R0330_15	FRA-6	FRA-6	2.11	2.11
GEV206_R0330_16	FRA-6	FRA-6	2.11	2.11
GEV206_R0330_17	FRA-6	FRA-6	2.11	2.11

Table 1: Strain gage properties for UD specimens with fibers at 30°.

The dimensions of the specimens are given in Table 2. The thickness and the width were measured with a digital calliper rule with 0.01 mm precision. Three measurements were performed: one in the middle and one near each end-tab. Average width and thickness were calculated and the resulting load bearing area was calculated.

	width (mm)				thickness (mm)				area (mm2)
	a	b	c	Av.	a	b	c	Av.	Av.
GEV206_R0330_12	24.41	24.40	24.40	24.40	3.85	3.84	3.86	3.85	93.95
GEV206_R0330_13	24.48	24.49	24.51	24.49	3.77	3.78	3.82	3.79	92.83
GEV206_R0330_14	24.47	24.48	24.49	24.48	3.89	3.85	3.90	3.88	94.98
GEV206_R0330_15	24.54	24.49	24.44	24.49	3.84	3.86	3.87	3.86	94.45
GEV206_R0330_16	25.09	25.13	25.11	25.11	3.86	3.84	3.84	3.85	96.59
GEV206_R0330_17	24.20	24.28	24.34	24.27	3.84	3.89	3.89	3.87	94.02

Table 2: Dimensions of UD GEV206 specimens with fibers at 30°.

1.2. Test results

The orientation of the strain gauges on the 30° off-axis specimen is shown in Figure 1. The x- and y-axes are orientated in the loading direction; the 1 and 2-axes are orientated in the fiber direction.

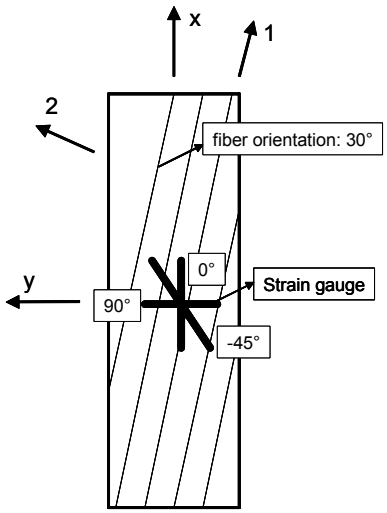

Figure 1: Axes in 30° off-axis specimen.

The failure shear stresses τ_{12}, failure shear strain γ_{12} and shear modulus G_{12} are given in Table 3 for the tested specimens. The failure shear strains γ_{12} are calculated as follows:

$$\gamma_{12} = -2mn\varepsilon_x + 2nm\varepsilon_y + (m^2 - n^2)\gamma_{xy}$$

The failure shear stress τ_{12} is calculated out of the tensile failure stress as follows:

$$\tau_{12} = -mn\sigma_x \text{ with } m = \cos\vartheta \text{ and } n = \sin\vartheta.$$

The shear modulus is calculated out of the shear stress and shear strain for strains between 0.05% and 0.25%. For some files the value of 0.25% was not reached for the first loading cycle, so strains were calculated until the maximum obtained strain value for that first cycle. Average values and standard deviations are calculated.

Coupon ID number	Failure shear stress τ_{12} (MPa)	Failure shear strain γ_{12} (%)	Shear modulus G_{12} (Gpa)
GEV206_R0330_12	55.57	2.25	8.95
GEV206_R0330_13	52.54	2.18	8.17
GEV206_R0330_14	53.28	2.38	6.14
GEV206_R0330_15	54.04	2.34	7.91
GEV206_R0330_16	51.40	2.80	6.34
GEV206_R0330_17	51.24	1.80	7.20
Average	53.01	2.29	7.45
Standard dev.	1.65	0.32	1.10

Table 3: Experimental results from static tensile GEV206-R0330 tests.

For more detailed results concerning the 30° off-axis tests performed at the VUB, we refer to report OB_TG3_R011 (document number 10149) on the Optimat Blade website.

2. Resonalyser

2.1. Principle

The Resonalyser procedure is a mixed numerical / experimental technique for the identification of the orthotropic engineering constants by the measurement of the vibration behaviour of rectangular test plates. The method results in averaged values over the whole plate area. With one test all four engineering constants are determined non-destructively, which gives several advantages with regard to classical testing. The visco-elastic behaviour of orthotropic materials in a plane state of stress can be characterised by four independent engineering constants. The constants appear as complex values in the compliance matrix that describes the relation between the strain column and stress column:

$$\begin{Bmatrix} \varepsilon_1^* \\ \varepsilon_2^* \\ \gamma_{12}^* \end{Bmatrix} = \begin{bmatrix} \frac{1}{E_1^*} & -\frac{\nu_{12}^*}{E_2^*} & 0 \\ -\frac{\nu_{21}^*}{E_1^*} & \frac{1}{E_2^*} & 0 \\ 0 & 0 & \frac{1}{G_{12}^*} \end{bmatrix} \begin{Bmatrix} \sigma_1^* \\ \sigma_2^* \\ \tau_{12}^* \end{Bmatrix}$$

The used symbols are:

ε_i^*	: normal strain component in the i-direction
γ_{12}^*	: shear strain component in the 12-plane
σi^*	: normal stress component in the i-direction
τ_{12}^*	: shear stress component in the 12-plane
ν_{ij}^*	: Poisson's ratio in the ij-plane
E_i^*	: Young's modulus in the i-direction
G_{12}^*	: Shear modulus in the 12-plane

The complex engineering constants can be written as:

$E_1^* = E_1.[\ 1 + i.tg(E_1)\ ]$
$E_2^* = E_2.[\ 1 + i.tg(E_2)\ ]$
$\nu_{12}^* = \nu_{12}.[\ 1 + i.tg(\nu_{12})\ ]$
$G_{12}^* = G_{12}.[\ 1 + i.tg(G_{12})\ ]$

The real part of the engineering constants describes the pure elastic behaviour of the material while the imaginary part describes the dissipative or damping behaviour. The dissipative part is often called 'the tangents delta'. The characterisation of orthotropic material hence requires the evaluation of 8 independent constants: 4 real values and 4 'tangents delta' values.

The resonalyser procedure proceeds in two parts: the first part is the evaluation of the real part of the engineering constants using measured resonant frequencies and the second part determines the imaginary part by measured modal damping ratios. The second part is optional and is only executed by people who are also interested in the damping behaviour of the examined material. In this report only the real part of the engineering constants will be determined.

2.1.1. Estimation of the real part of the engineering constants

The principle for the determination of the real part is to compare measured resonant frequencies of a rectangular test plate with frequencies computed with a numerical model of the test plate. This principal is illustrated in Figure 2.

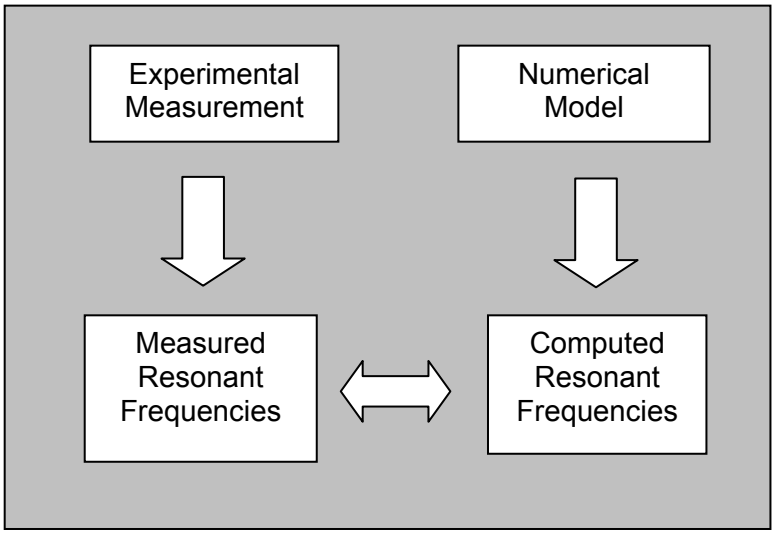

Figure 2: The principle for the identification of the real part of the engineering constants.

A thin plate model based on the Love Kirchhoff theory is used for the numerical model of the test plate. Extensions of the Resonalyser procedure use thick plate models with linear and higher order shear corrections [1]. The resonant frequencies and modeshapes of the numerical model can be found by the solution of an eigenvalue problem.

The parameter column contains the 4 real parts of the orthotropic engineering constants:

$$\{p\} = \begin{Bmatrix} E_1 \\ E_2 \\ G_{12} \\ \nu_{12} \end{Bmatrix}$$

Starting from an initial value, the parameters are iteratively updated. This yields good results if the parameters can be observed through the measured resonant frequencies. This means that at least one measured resonant frequency in the selected measurement set must sufficiently change for variations of each of the 4 parameters.

It can be shown [2] that this demand requires a length/width ratio a/b of the test plate close to the value given by:

$$\frac{a}{b} = \sqrt[4]{\frac{E_1}{E_2}}$$

The preparation of such a plate requires the knowledge of the ratio E_1 / E_2. The value of this ratio can be found by cutting two test beams in perpendicular directions from the test plate. The

measurement of the fundamental (first) resonant frequencies f_{B1} and f_{B2} of this two beams allows the determination of E_1 and E_2 and hence of the ratio a/b. The remaining two constants ν_{12} and G_{12} are to be identified exclusively by resonant frequencies of the adjusted test plate. A freely suspended rectangular plate with the right dimensions shows a first mode shape in torsion and next a anticlastic and a synclastic mode shape as shown in Figure 3.

The stress pattern of the torsion mode shape is dominated by shear stresses and hence the associate frequency f_{P1} is very sensitive for variations of G_{12}. The anticlastic (saddle mode) and the synclastic (breathing mode) mode shapes both show the same stress pattern but with opposite sign of the normal stress ratio. The difference between the associates frequencies f_{P3} and f_{P2} is only due to the value of Poisson's ratio. For the (theoretical) case of zero Poisson's value, both mode shapes have the same resonant frequency.

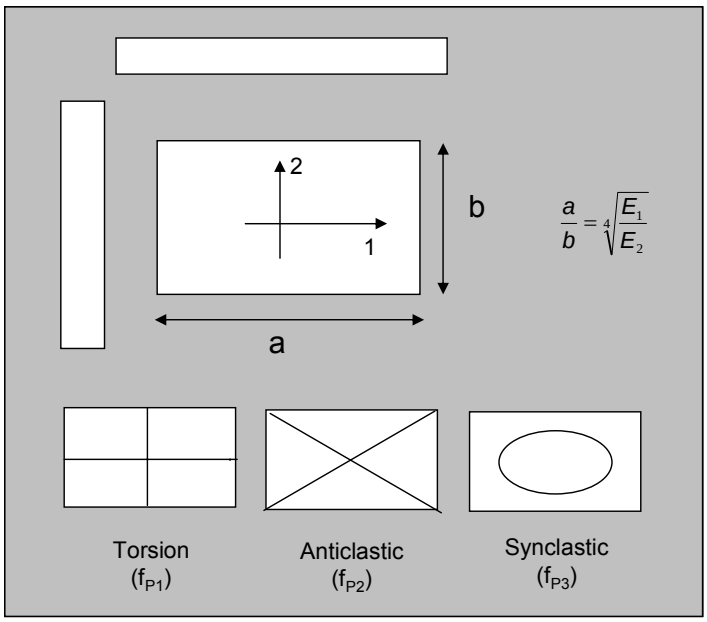

Figure 3: Two test beams and the adjusted test plate.

These phenomena provide an easy way of finding good starting values for G_{12} and ν_{12}:

$$\begin{Bmatrix} G_{12}^{Initial} \\ \nu_{12}^{Initial} \end{Bmatrix} = \begin{bmatrix} S_{G12} & 0 \\ 0 & S_{\nu 12} \end{bmatrix}^{-1} \begin{Bmatrix} \lambda_1 \\ \lambda_3 - \lambda_2 \end{Bmatrix}$$

in which:

λ_1 : The first eigenvalue ($\lambda_1 = (2\pi f_{P1})^2$)
λ_2 : The second eigenvalue ($\lambda_2 = (2\pi f_{P2})^2$)
λ_3 : The third eigenvalue ($\lambda_3 = (2\pi f_{P3})^2$)
S_{G12} : The sensitivity of the torsion eigenvalue for G_{12} variations
$S_{\nu 12}$: The sensitivity of the difference of the synclastic and anticlastic eigenvalues for variations of Poisson's ratio v12.

The identification of the elastic parts of the engineering constants is performed using the two beam frequencies and the three plate frequencies:

$$\{m\} = \begin{Bmatrix} f_{B1} \\ f_{B2} \\ f_{P1} \\ f_{P2} \\ f_{P3} \end{Bmatrix} \qquad \text{and} \qquad \{p^{(0)}\} = \begin{Bmatrix} E_1^{Initial} \\ E_2^{Initial} \\ G_{12}^{Initial} \\ \nu_{12}^{Initial} \end{Bmatrix}$$

The computed frequencies are updated until they match the observed frequencies {m}. The (5 x 4) sensitivity matrix [S] is:

$$[S] = \begin{bmatrix} S^{Beam1} & 0 & 0 & 0 \\ 0 & S^{Beam2} & 0 & 0 \\ S_{11}^{plate} & S_{12}^{plate} & S_{13}^{plate} & S_{14}^{plate} \\ S_{21}^{plate} & S_{22}^{plate} & S_{23}^{plate} & S_{24}^{plate} \\ S_{31}^{plate} & S_{32}^{plate} & S_{33}^{plate} & S_{34}^{plate} \end{bmatrix}$$

The sensitivity of the plate frequency (i) for variations of the parameter (j) is recomputed in every iteration step [2]:

$$S_{ij}^{Plate} = \{\phi\}_i^{\tau} \frac{\partial [K^{Plate}]}{\partial p_j} \{\phi\}_i$$

in which $\{\phi\}i$ is the i-th modeshape and K^{Plate} is the stiffness matrix of the numerical model of the test plate (both computed with the value of the parameters at a specific iteration step). The sensitivity of a freely suspended thin beam frequency for variations of the Young's modulus S^{Beami} can be found easily from the following relations:

$$f_{Bi} = \frac{22.4}{L^2}\sqrt{\frac{E_i I}{\rho A}} \qquad \text{thus} \qquad \frac{\partial f_{Bi}}{\partial E_i} = \frac{11.2}{L^2}\sqrt{\frac{I}{\rho A E_i}}$$

(EI is the bending stiffness, ρA the weight per unit length, L the beam length)

The parameter value in the final iteration is the result of the first stage of the resonalyser procedure, determining the real part of the engineering constants.

2.1.2. Estimation of the complex part of the engineering constants

The complete identification of the complex moduli requires also the knowledge of the imaginary (or dissipative) part of the engineering constants. In the orthotropic case this includes the determination of 4 tangents delta. The (4x1) parameter column for the second stage hence is:

$$\{p\} = \begin{Bmatrix} tg(E_1) \\ tg(E_2) \\ tg(G_{12}) \\ tg(\nu_{12}) \end{Bmatrix}$$

These tangents values can be identified by the measurement of the modal damping ratios associated with the 2 beam and the 3 plate resonant frequencies. The modal damping ratios can be evaluated by curve fitting the decaying sinusoidal signal in the time domain after an excitation of the test specimen with the envisaged resonant frequencies as shown in Figure 4.

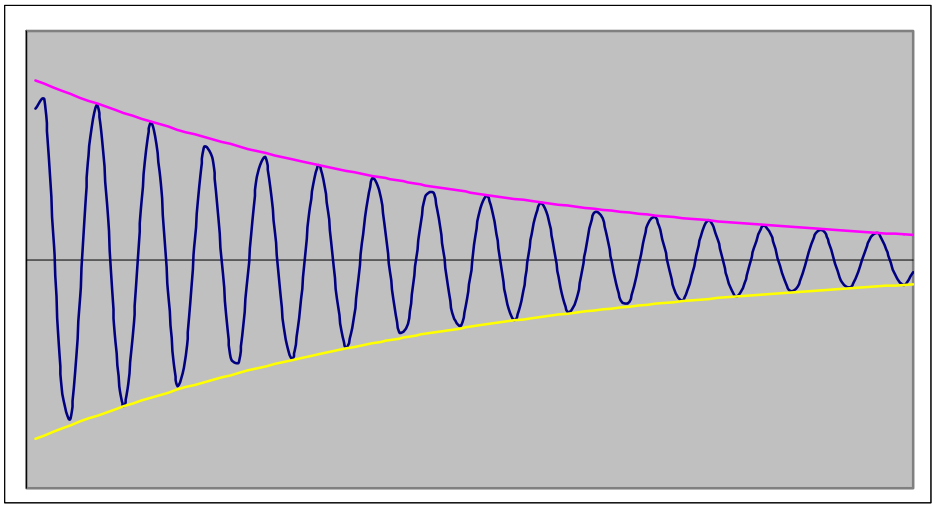

Figure 4: A freely decaying signal in the time domain at a resonant frequency.

The signal is curve fitted with the formula:

$$x(t) = Xe^{-\xi\omega t}\sin(\omega t - \varphi)$$

in which ξ is the modal damping ratio and ω is the circular resonant frequency ($\omega = 2\pi f$).

The curve fitting in the time domain allows obtaining accurate results even for lightly damped test specimen. The main problems for the measurement of the modal damping ratios are situated on the experimental level. Small variations in the boundary conditions (suspension threats, accelerometer wiring ...) induce external damping that can not be distinguished from the internal material damping. Therefore it is strongly preferred to generate and measure the signals without physical contact. The excitation can be performed acoustically with a loudspeaker and the measurement of the decaying signal can be done with a laser vibrometer.

The influence of the boundary conditions can be minimised by the suspension of the test specimen in nodal points of the mode shapes as shown in Figure 5.

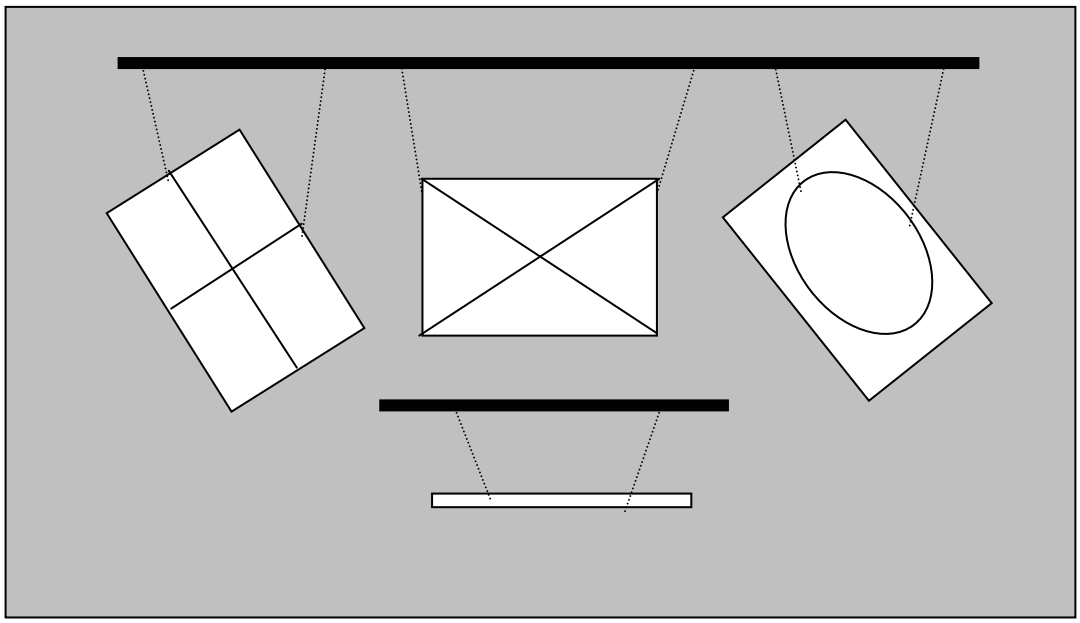

Figure 5: Suspension in nodal points of the test specimen.

A simplifying element in the second stage is that the relation between the parameters and the measured modal damping ratios is linear:

$$2\xi_{fB1} = tg(E_1)$$
$$2\xi_{fB2} = tg(E_2)$$
$$2\xi_{fP1} = w_{11}.tg(E_1) + w_{12}.tg(E_2) + w_{13}.tg(\nu_{12}) + w_{14}.tg(G_{12})$$
$$2\xi_{fP2} = w_{21}.tg(E_1) + w_{22}.tg(E_2) + w_{23}.tg(\nu_{12}) + w_{24}.tg(G_{12})$$
$$2\xi_{fP3} = w_{31}.tg(E_1) + w_{32}.tg(E_2) + w_{33}.tg(\nu_{12}) + w_{34}.tg(G_{12})$$

The coefficients w_{ij} can be computed with the numerical plate model from the modal strain distributions and modal damping energy expressions [3].

The sensitivity matrix [S] can be derived easily:

$$[S] = \left[\frac{\partial y}{\partial p}\right] = \frac{1}{2}.\begin{bmatrix} 1 & 0 & 0 & 0 \\ 0 & 1 & 0 & 0 \\ w_{11} & w_{12} & w_{13} & w_{14} \\ w_{21} & w_{22} & w_{23} & w_{24} \\ w_{31} & w_{32} & w_{33} & w_{34} \end{bmatrix}$$

The (5x1) measurement column {m} is:

$$\{m\} = \begin{Bmatrix} \xi_{fB1} \\ \xi_{fB2} \\ \xi_{fP1} \\ \xi_{fP2} \\ \xi_{fP3} \end{Bmatrix}$$

The linear character of the equation allows starting from arbitrary initial values for the parameters. They can thus be taken all as zero. The least squares estimator can be used with $\{p\}^0 = 0$ and $\{y\}^0 = 0$ and will yield immediately the optimal parameter values:

$$p_k^{(opt)} = [S_{sk} S_{sm}]^{-1} S_{rm} . m_r$$

This explanation about the estimation of the complex part of the engineering constants is only given for information. Only the real part of the engineering constants is determined experimentally in this report.

2.1.3. Practical procedure

The above described Resonalyser procedure is automated using a MS-windows PC programme. The PC is equipped with a data acquisition card. The practical measurement procedure proceeds as follows:

1. Machine two test beams from the original test plate as indicated in Figure 3
2. Measure the first resonant frequency of both test beams and compute initial values for E1 and E2
3. Determine the dimensions of the test plate and machine the test plate
4. Measure the first 3 frequencies of the test plate
5. Start the first stage of the Resonalyser procedure for the identification of the real parts of the engineering constants
6. Measure the modal damping ratios associated with the measured frequencies of the test beams and plate
7. Start the second stage of the Resonalyser procedure for the identification of the imaginary parts of the engineering constants

At the end of the procedure the complete set of orthotropic complex engineering constants are identified. In this report only steps 1 till 5 will be performed to determine the real parts of the engineering constants.

2.1.4. Error discussion

In the Resonalyser procedure the estimation of the real part is based on the measurement of resonant frequencies. The experimental error on measured frequencies is small, even if non-sophisticated measurement equipment is used. The results of the mixed numerical-experimental method for material parameter idenficiation (MMM) with high quality test plates (homogeneous elastic properties and constant thickness and thus an accurate numerical model) are accurate. A detailed error discussion on the real part errors can be found in [2].

The estimation of the complex part is based on the measurement of the modal damping ratios. This part is more sensitive to measurement noise and non-linear behaviour of the damping as a function of the excitation amplitude. The results are hence less accurate. A detailed discussion on the complex part errors can be found in [3, 4].

More examples of MMM procedures on different physical problems can be found in [5, 6].

2.2. Set-up

Two plates were delivered at the VUB with indication PL102. We renamed them as PL102/1 and PL102/2. Plate 102/1 was used for the tests with the Resonalyser. Two beams were cut from the plate, one in the direction of the fibers (with name L1) and one perpendicular to the fibers (T1) as indicated on Figure 6. These names L and T refer to longitudinal and transverse direction. After the testing of the beams, the ratio for the Poisson plate is known and was cut from the plate (P1). The rest of the plate is used for the torsion tests as will be described in the next paragraph.

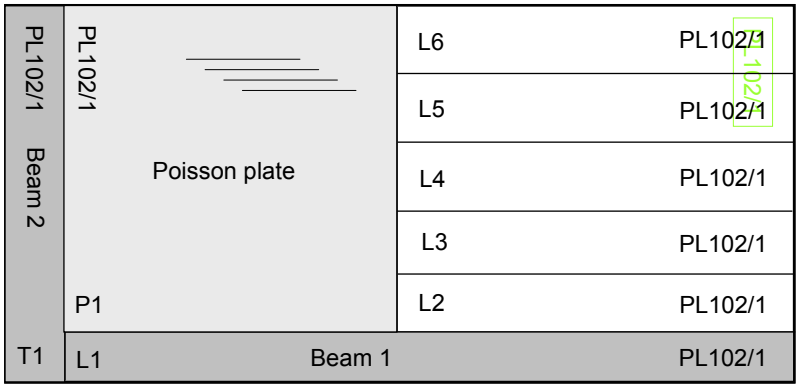

Figure 6: Identification of beams and Poisson plate cut from plate PL 102/1.

The set-up is shown in Figure 7. The beams and plate are suspended simulating free boundary conditions since they are fixed only in the points with zero displacements during resonance.

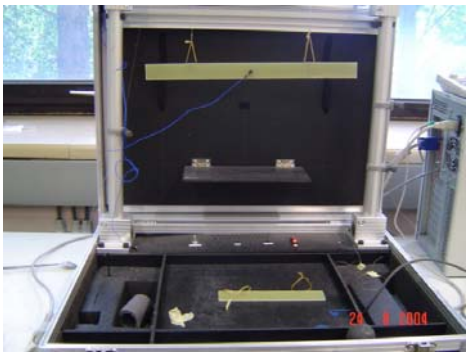

a) Beam 1 (L1)

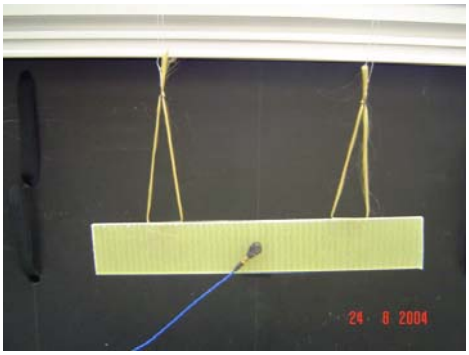

b) Beam 2 (T1)

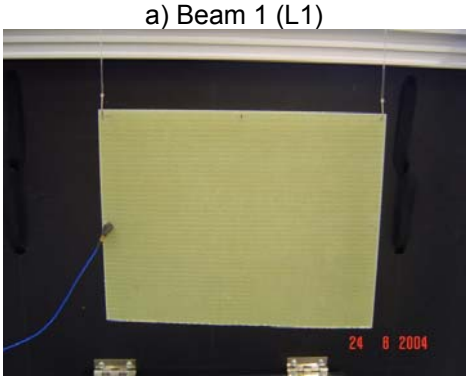

c) Poisson plate (P1) saddle mode

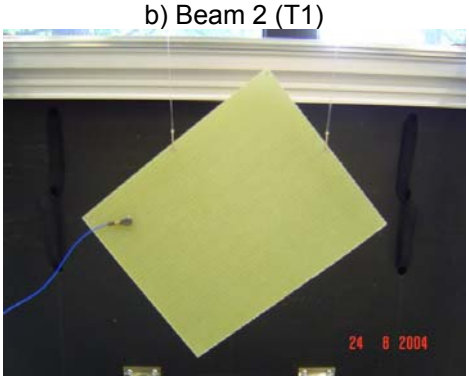

d) Poisson plate (P1) torsion mode/breathing mode

Figure 7: Suspension of beams and plate causing free boundary conditions.

The dimensions (length, width and thickness) and the mass of the beams and plate are given in Table 4. Thickness measurements were obtained with two methods.

	length (mm)	width (mm)	thickness micrometer (mm)	thickness dry/wet mass (mm)	mass (g)
Beam 1 //	415.00	30.25	3.65	3.56	87.94
Beam 2 ⊥	189.88	30.01	3.69	3.58	39.80
Plate torsion	198.55	156.96	3.68	3.57	212.22
Plate saddle					
Plate breathing					

Table 4: Dimensions and mass of the tested beams and plate.

The thickness measurements need to be very accurate using this Resonalyser technique since up till a third power of the thickness is used in the formulas. Therefore thickness measurements were performed both with a micrometer and with calculating the thickness from the dry and wet mass. The thickness measurements with the micrometer were performed at 3 different places for the beams and at 16 places for the plate. Average values were calculated afterwards. The measured thickness with the micrometer is always higher than the one calculated with the mass. This may be due to the fact that the surface of the specimens is not completely flat. Small roughness of the surface exists due to the fabrication procedure as illustrated in Figure 8. This gives higher measured thickness values with the micrometer than the real thickness. The thickness values calculated by using the mass of a dry and a specimen in water may be lower than the real thickness since air bubbles can occur around the specimen. The real thickness will probably be between the both values.

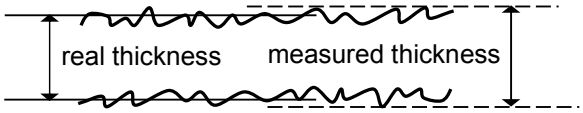

Figure 8: Thickness of a specimen with rough surface.

Although the difference in thickness is small between the two methods, the finally obtained engineering constants can differ substantially. For other tests as for instance tension tests, this small difference in thickness has less influence since only the first power of the thickness is used for calculating the Young's modulus.

2.3 Results

The measured resonant frequencies for the two beams and the first three resonant frequencies for the plate are given in Table 5.

	frequency (Hz)
Beam 1 //	92.38
Beam 2 ⊥	282.03
Plate torsion	205.4
Plate saddle	390.8
Plate breathing	444.9

Table 5: Measured frequencies of the tested beams and plate.

The resulting engineering constants are listed in Table 6. The first column shows the results for the thickness measured with a micrometer; the second column for the thickness calculated from the dry mass and mass under water. The difference between the two results is not negligible.

	Thickness micrometer	Thickness dry/wet mass
E_1 (GPa)	35.2	38.1
E_2 (GPa)	14.2	15.6
G_{12} (GPa)	5.21	5.71
ν_{12} (-)	0.314	0.310
ν_{21} (-)	0.127	0.127

Table 6: Obtained engineering constants with thickness measured with micrometer and thickness measured with dry mass and mass in water.

The resulting plate stiffnesses are listed in Table 7. Again the first column shows the results for the thickness measured with a micrometer; the second column for the thickness calculated from the dry mass and mass under water.

	Thickness micrometer	Thickness dry/wet mass
D_{11} (Pa)	152.191	150.358
D_{22} (Pa)	61.376	61.591
D_{12} (Pa)	19.254	19.121
D_{66} (Pa)	21.638	21.645

Table 7: Obtained plate stiffnesses with thickness measured with micrometer and thickness measured with dry mass and mass in water.

2.4 References

[1] Hua, H., “Identification of Plate Rigidities of Anisotropic Rectangular Plates, Sandwich Panels and Orthotropic Circular Disks using Vibration Data”, *Ph.D. Thesis presented at the Vrije Universiteit Brussel, Belgium,* 1993.

[2] Sol, H., “Identification of anisotropic plate rigidities using free vibration data”, *Ph.D.Thesis presented at the Vrije Universiteit Brussel, Belgium,* 1986

[3] Sol, H., Hua, H., De Visscher, J., Vantomme, J., De Wilde, W.P., “A Mixed Numerical/Experimental technique for the nondestructive identification of the Stiffness Properties of fibre reinforced Composite Materials”, Journal of NDT&E International, Vol. 30, N°2, pp.85-91, Elsevier Science Ltd, 1997

[4] Sol, H. et all., “La procedure resonalyser, *La revue des laboratoires d'Essais*“, n° 46, pp.10-12, 1996

[5] Cardon, A.H., Sol, H., De Wilde, W.P., De Visscher, J., Hoes, K., Dinescu, D. “Mixed numerical - experimental techniques: past, present and future”, Published in "Recent Advances in Experimental Mechanics", E.E. Gdoutos (ed.), Kluwer Academic Publishers, ISBN 1-4020-0683-7, 2002, chapt. Hybrid methods, pp. 551 – 560, october 2002

[6] Sol, H. & Oomens, C., “Material Identification Using Mixed Numerical Experimental Methods”, *Kluwer Academic Publishers,* 1997

3. Torsion tests

3.1. Principle [1, 2]

The definition of the dimensions used in the following formulas is according to the designation of Figure 9.

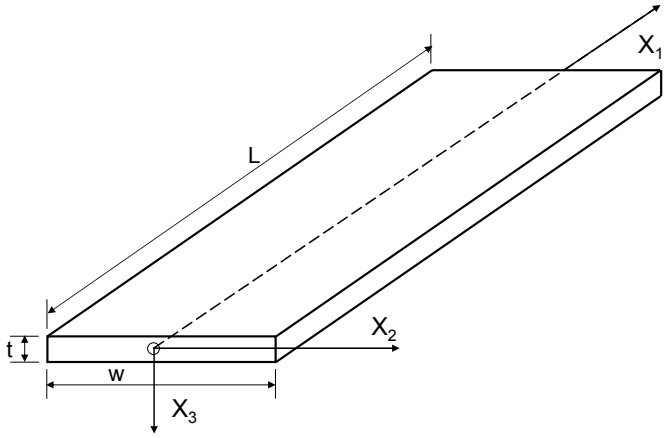

Figure 9: Designation of axis system.

The equation relating the applied torque M_T to the angle of twist per unit of length θ/L for an isotropic rectangular flat beam within the linear elastic range is:

$$M_T = \beta w t^3 G_{12} \frac{\theta}{L}$$

where $$\beta = \frac{1}{3}\left(1 - \frac{192}{\pi^5}\frac{t}{w}\right) \sum_{n=1.3.5}^{\infty} \frac{1}{n^5} \tanh\frac{n\pi w}{2t}$$

For small values of w/t this equation can be simplified in the following form due to the fact that the tanh ($n\pi w/2t$) becomes almost equal to one:

$$M_T = \frac{1}{3} G w t^3 \left(1 - 0.63\frac{t}{w}\right)\frac{\theta}{L}$$

For an orthotropic rectangular bar the relation between torque and torsion angle becomes:

$$M_T = \beta(c) w t^3 G_{12} \frac{\theta}{L}$$

where $\beta = \frac{32c^2}{\pi^4} \sum_{n=1.3.5}^{\infty} \frac{1}{n^4}\left(1 - \frac{2c}{n\pi}\tanh\frac{n\pi}{2c}\right)$ and $c = \frac{w}{t}\sqrt{\frac{G_{13}}{G_{12}}}$

with G_{12} being the in-plane shear modulus and G_{13} the out-of-plane shear modulus. By combining the measurements of two bars with different width, it is possible to compute the in-plane, as well as the out-of-plane shear modulus:

TEST 1 w_1, t_1, L_1 $\rightarrow$ $M_T^1 = \beta(c_1) w_1 (t_1)^3 G_{12} \frac{\theta_1}{L_1}$

linear regression $\rightarrow$ $M_T^1 = a_1 \frac{\theta_1}{L_1}$

TEST 2 w_2, t_2, L_2 $\rightarrow$ $M_T^2 = \beta(c_2) w_2 (t_2)^3 G_{12} \frac{\theta_2}{L_2}$

linear regression $\rightarrow$ $M_T^2 = a_2 \frac{\theta_2}{L_2}$

combining the two equations results in:

$$\frac{a_1}{a_2} = \frac{G_{12}\beta(c_1) w_1 (t_1)^3}{G_{12}\beta(c_2) w_2 (t_2)^3}$$

when defining $\alpha = \frac{c_2}{c_1} = \frac{w_2 / t_2}{w_1 / t_1} = \frac{w_2 t_1}{w_1 t_2}$, we have $\frac{w_2 (t_2)^3}{w_1 (t_1)^3} a_1 \beta(\alpha c_1) - a_2 \beta(c_1) = 0$

We can now solve the equation for c_1 and use:

$$G_{12} = \frac{a_1}{\beta(c_1) w_1 (t_1)^3}$$

to obtain the in-plane shear modulus G_{12}

and $$c = \frac{w}{t}\sqrt{\frac{G_{13}}{G_{12}}}$$

to calculate the out-of-plane shear modulus G_{13}.

In order to be able to combine more than two different widths, a Smith least square fit of the following function was programmed:

$$\frac{a_i}{w t^3} = G_{13}\beta\left(\frac{w}{t}\sqrt{\frac{G_{13}}{G_{12}}}\right)$$

where a_i is the first order coefficient of the linear regression relating torque and torsion angle of each experiment.

3.2. Set-up

A torsion bench was constructed at the department of Mechanics of Materials and Constructions of the Free University of Brussels. It consists of a stepping motor with a planetary gearbox so that for one step an angular rotation of 0.036 degrees is obtained. The maximum torque which can be applied is 25Nm. A torque cell measures the applied torque up to 26Nm with a minimum resolution of 4Nmm. The construction is such that one end is completely free to move so that no tensile forces can be introduced. The rotation angle and the corresponding torque are acquired by a data acquisition board and recorded on a hard disc of a PC. The experimental setup is illustrated in Figure 10.

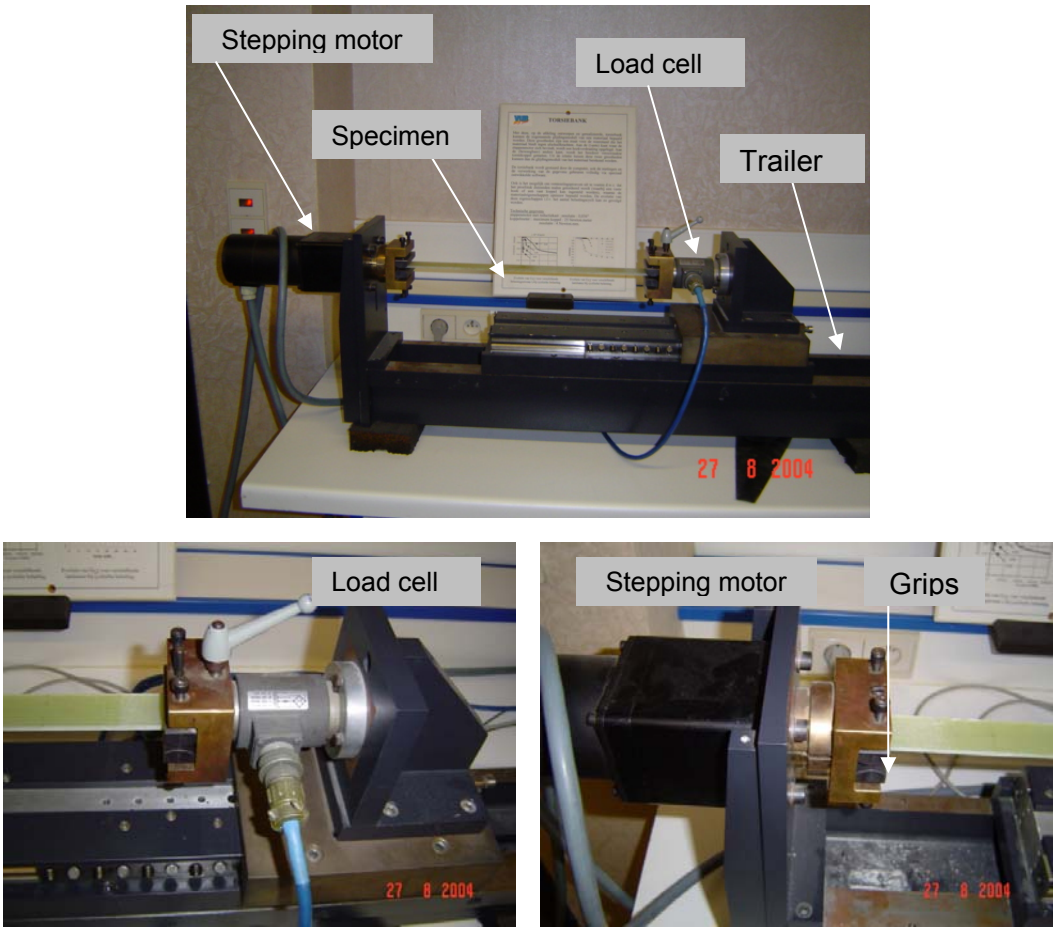

Figure 10: Torsion bench with identification of different parts.

The material tested was OB UD plate material with four layers. Two plates of this material were delivered at the VUB with indication PL102. We renamed them as PL102/1 and PL102/2. Plate 102/1 was used for the tests with the Resonalyser (indicated with grey colours) and for these torsion tests. Plate 102/2 was used for these torsion tests too. Only the in-plane shear properties G_{12} were studied.

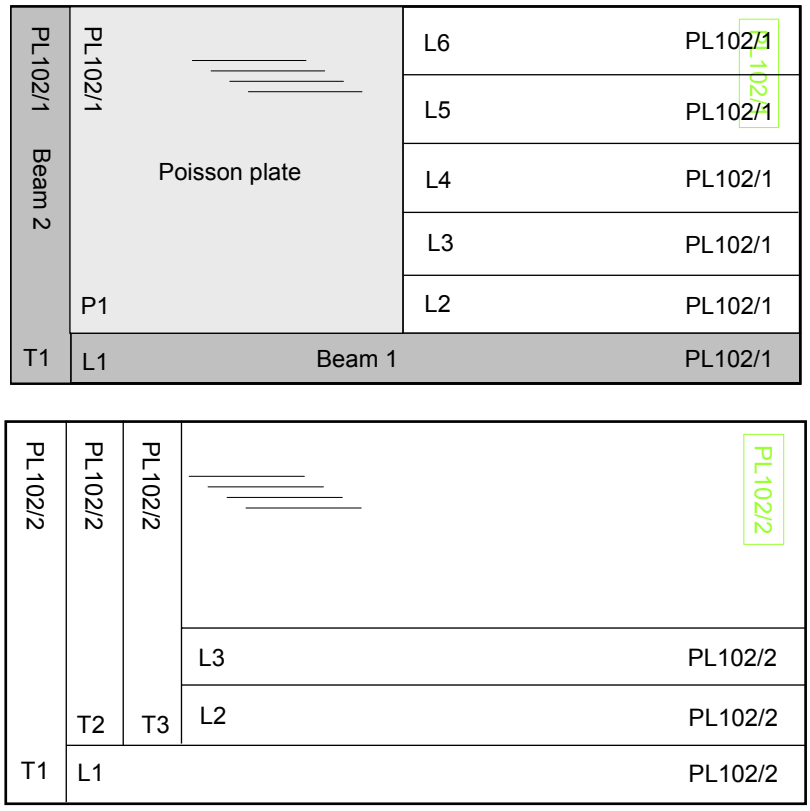

Figure 11: Identification of beams and Poisson plate cut from plate PL 102/1 and PL 102/2.

In Table 8 the dimensions of the tested beams are given. The length is not the length of the beams, but the length between the two grips during the test. For this kind of tests the thickness is again very important since a third power of the thickness occurs in the used formulas. Therefore thickness measurements were performed both with a micrometer and with calculating the thickness from the dry and wet mass as explained in the paragraph about the Resonalyser. Three beams with different lengths were tested for each plate

	width (mm) average	tested length (mm) average	thickness (mm) micrometer	thickness (mm) dry/wet mass
plate 102/1				
L1 (beam 1 //)	30.25	401.50	3.65	3.56
L2	30.09	204.15	3.59	3.55
L3	30.11	191.50	3.62	3.55
plate 102/2				
L1	30.47	402.00	3.66	3.61
L2	30.28	336.00	3.67	3.61
L3	30.38	335.00	3.62	3.58

Table 8: Dimensions of tested beams from plate 102/1 and 1202/2.

3.3. Results

		between:	thickness with micrometer	thickness with dry/wet mass
Plate 102/1	L1 (401.50mm)	0.5° and 4°	4.99	5.36
		0.5° and 3°	4.99	5.36
		1° and 3°	5.00	5.39
		0.84° and 6.72°	4.93	5.30
		0.84° and 5.04°	4.97	5.34
		1.68° and 5.04°	4.96	5.34
		1° and 8°	4.91	5.28
		1° and 6°	4.94	5.32
		2° and 6°	4.92	5.29
	L2 (204.15mm)	0.5° and 4°	5.03	5.20
		0.5° and 3°	5.05	5.22
		1° and 3°	5.06	5.23
	L3 (191.50mm)	0.5° and 4°	5.14	5.44
		0.5° and 3°	5.16	5.46
		1° and 3°	5.17	5.47
Plate 102/2	L1 (402.00mm)	0.5° and 4°	5.01	5.21
		0.5° and 3°	5.01	5.21
		1° and 3°	5.02	5.23
		0.84° and 6.72°	4.94	5.14
		0.84° and 5.04°	4.98	5.19
		1.68° and 5.04°	4.97	5.17
		1° and 8°	4.92	5.12
		1° and 6°	4.96	5.16
		2° and 6°	4.93	5.13
	L2 (336.00mm)	0.5° and 4°	5.02	5.27
		0.5° and 3°	5.03	5.28
		1° and 3°	5.04	5.28
		0.84° and 6.72°	4.95	5.19
		0.84° and 5.04°	4.99	5.24
		1.68° and 5.04°	4.98	5.22
	L3 (335.00mm)	0.5° and 4°	5.33	5.51
		0.5° and 3°	5.34	5.52
		1° and 3°	5.36	5.53
		0.84° and 6.72°	5.26	5.43
		0.84° and 5.04°	5.30	5.48
		1.68° and 5.04°	5.29	5.46
	Average		5.05	5.30
	Standard dev.		0.13	0.12

Table 9: Shear modulus results obtained with torsion tests.

The shear modulus was calculated between different intervals of rotation angle to judge the linearity of the results. For a length of about 200mm, the chosen intervals were 0.5°-4°, 0.5°-3° and 1°-3°. For longer lengths, the corresponding angles were adapted by using a linear law since for longer lengths, higher rotation angle are obtained for the same applied torque. For lengths of 335mm, the corresponding intervals were 0.84°-6.72°, 0.84°-5.04° and 1.68°-5.04° and for lengths of 400mm the intervals were 1° -8°, 1°-6° and 2°-6°. For information the results for the longer lengths were also calculated with the smaller angles. You can see an important difference between the results calculated with a thickness measured with a micrometer and calculated from the dry mass and the mass under water. Also higher lengths seem to give lower shear modulus results. This was expected since the stiffness of the part of the specimen beyond the grips has a higher influence for shorter specimens. Actually a correction should be made for all results to take the stiffness of this small part of material into account.

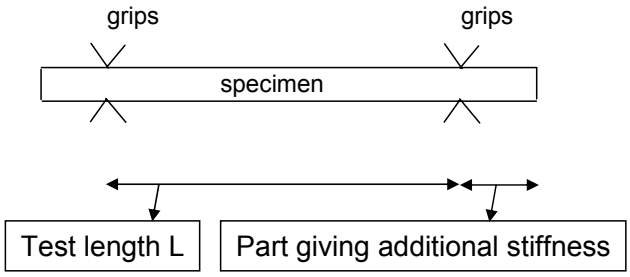

Figure 12: Influence of length beyond clamps.

3.4 References

[1] Van Hemelrijck, D., Schillemans, L., De Roey, F., Daerden I., Boulpaep, F., Cardon, A., "A computerized test set-up for the determination of the in-plane and out-of-plane shear modulus in orthotropic specimens", Mechanical identification of composites edited by Vautrin, A., Sol, H., Proceedings of the European Mechanics colloquium 269, 1990, pp.149-155.

[2] Van Hemelrijck, D., "Materiaalkarakterisatie van vezelversterkte composietmaterialen", *Thesis presented at the Vrije Universiteit Brussel, Belgium,* 1984

4. Comparison between shear results performed at VUB, UP and at RISOE

4.1 Results of tests performed at RISOE

4.1.1 30° off-axis tests performed at Risoe

Results of failure shear stresses, failure shear strains and of shear moduli obtained by Risoe with 30° off-axis tests are shown in Table 10.

	Failure shear stress τ12 (MPa)	Failure shear strain γ12 (%)	shear modulus (Gpa)
GEV206-I01-30-2	47.87	0.954	7.19
GEV206-I01-30-3	49.22	1.157	8,57
GEV206-I01-30-4	49.5	1.128	8.51
GEV206-I01-30-5	50.67	1.308	8.52
GEV206-I01-30-6	50.67	1.888	9.17
GEV206-I01-30-7	50.76	1.362	9.72
Average	49.78	1.30	8.62
Standard dev.	1.15	0.32	0.85

Table 10: Failure stresses, failure strains and shear modulus obtained by Risoe on 30°-off axis specimens.

These results were found in report OB_TG3_R010 (document number 10147) on the Optimat Blade website written by Risoe, where you can also find more detailed information about these results, the used specimen type and the test procedure.

4.1.2 V-notched tests performed at Risoe

Results of failure shear stresses, failure shear strains and of shear moduli obtained by Risoe with V-notched tests are shown in Table 11.

	Failure shear stress τ12 (MPa)	Failure shear strain γ12 (%)	Shear modulus (Gpa)
GEV206-I04-00-31	84	7.82	8.5
GEV206-I04-00-32	83	8.08	8.4
GEV206-I04-00-33	82	7.78	8.9
GEV206-I04-00-34	80	7.67	8.6
GEV206-I04-00-46	77	7.97	4.8
GEV206-I04-00-47	83	7.89	7.1
GEV206-I04-00-48	83	7.93	5.3
Average	81	7.88	7.3
Standard dev.	2.43	0.13	1.69

Table 11: Failure stresses, failure strains and shear modulus obtained by Risoe on V-notched specimens.

These results were found in report OB_TG3_R009 (document number 10146) on the Optimat Blade website written by Risoe, where you can also find more detailed information about these results, the used specimen type and the test procedure.

4.2 Results of tests performed at UP

4.2.1 +/-45° tests performed at UP

Results of failure shear stresses, failure shear strains and of shear moduli obtained by UP with +/-45° tests are shown in Table 12.

	Failure shear stress $\tau 12$ (MPa)	Failure shear strain $\gamma 12$ (%)	Shear modulus (Gpa)
GEV208_I1000_0001	55.50	3.140	4.34
GEV208_I1000_0002	57.02	3.253	4.22
GEV208_I1000_0003	54.99	3.119	4.35
GEV208_I1000_0004	55.89	3.924	4.17
GEV208_I1000_0005	55.55	3.451	4.15
GEV208_I1000_0006	54.04	3.193	4.19
GEV208_I1000_0007	55.06	3.540	4.25
GEV208_I1000_0008	55.27	3.974	4.07
GEV208_I1000_0009	55.82	3.316	4.07
GEV208_I1000_0010	55.55	3.062	4.37
GEV208_I1000_0011	57.40	3.599	4.24
GEV208_I1000_0012	55.16	3.423	4.03
GEV208_I1000_0013	57.63	3.130	4.40
GEV208_I1000_0014	56.01	2.852	4.36
GEV208_I1000_0015	57.81	3.634	4.28
GEV208_I1000_0016	56.91	3.322	4.29
GEV208_I1000_0017	56.01	3.366	4.20
GEV208_I1000_0018	54.77	3.387	4.21
GEV208_I1000_0019	57.71		
GEV208_I1000_0020	57.45	3.600	4.23
GEV208_I1000_0021	57.23	3.231	4.27
GEV208_I1000_0022	56.32	3.776	4.03
GEV208_I1000_0023	54.35	2.912	4.27
GEV208_I1000_0024	55.66	3.347	4.28
GEV208_I1000_0025	57.25	3.480	4.32
GEV208_I1000_0027	55.47	3.613	4.23
Average	56.07	3.386	4.23
Standard dev.	1.10	0.28	0.10

Table 12: Failure stresses, failure strains and shear modulus obtained by UP on +/-45° specimens.

These results were found in report OB_TG2_R020 (document number 10207) on the Optimat Blade website written by UP, where you can also find more detailed information about these results, the used specimen type and the test procedure.

4.3. Comparison of the results and conclusions

In Table 13 a summary of all test results obtained with the different techniques at different institutes are shown, both for the average values and the standard deviations.

institute	type of test	average			standard deviation		
		failure shear stress τ_{12} (MPa)	failure shear strain γ_{12} (%)	shear modulus (GPa)	failure shear stress τ_{12} (MPa)	failure shear strain γ_{12} (%)	shear modulus (GPa)
VUB	30° off-axis	53.01	2.29	7.45	1.65	0.32	1.10
	resonalyser	-	-	5.21[(a)]	-	-	-
		-	-	5.71[(b)]	-	-	-
	torsion	-	-	5.05[(a)]	-	-	0.13
		-	-	5.30[(b)]	-	-	0.12
Risoe	30° off-axis	49.78	1.30	8.62	1.15	0.32	0.85
	V-notched	81.00	7.88	7.30	2.43	0.13	1.69
UP	+/-45°	56.07	3.39	4.23	1.1	0.28	0.1

(a) thickness measured with micrometer
(b) thickness measured with dry mass and mass in water

Table 13: Comparison of failure shear stress, failure shear strain and shear modulus obtained with different techniques.

The failure shear stresses obtained with V-notched tests are significantly higher than the failure shear stresses obtained with 30° off-axis tests and +/-45° tests. No failure shear stresses and strains could be obtained by the Resonalyser test, as this is just a non-destructive test to obtain the engineering constants. Also the torsion test is only suitable for determining shear moduli and not for determining accurately the failure strains and stresses. The failure shear stresses obtained with +/-45° tests are slightly higher than the failure shear stresses obtained by 30° off-axis tests where the values obtained with this technique by Risoe are slightly lower than the results obtained by VUB.

For the failure shear strains we can come to more or less the same conclusions as for the failure shear stresses. Again the values obtained with V-notched tests are significantly higher than the ones obtained with 30° off-axis tests and +/-45° tests. Now the failure strain values obtained with +/-45° tests for their part are significantly higher than the results obtained with 30° off-axis tests, which was not that obvious for the failure shear stresses. Also the difference between the failure strains obtained with the 30° off-axis tests performed at VUB and at Risoe is very large, where the results obtained at VUB are higher than the results obtained at Risoe and where the difference for the failure shear stresses was less high.

For the shear modulus, highest values are obtained by Risoe with the 30° off-axis tests. Results obtained by VUB with 30° off-axis tests are lower now, in contradiction to the failure stresses and failure strains which were higher. Shear moduli obtained with V-notched tests are of the same order as shear moduli obtained with 30° off-axis tests. Shear moduli obtained with Resonalyser test and torsion test are comparable, but much lower than the results obtained with V-notched tests and 30° off-axis tests. Results obtained with +/-45° tests are even lower however.

5. Conclusions

To conclude we can state that the shear results obtained with different techniques show significant differences. No clear conclusion can be made on the preference of one technique for appropriate determination of failure shear stresses, failure shear strains and shear moduli. Results obtained with V-notched tests seem to be too high, when compared with the other techniques for both failure strains and stresses, while results obtained with +/-45° seem to give low results for the shear modulus. For the failure stresses, results obtained with 30° off-axis tests and +/-45° tests are reasonably close to each other, while the results obtained with V-notched tests are too high. For the obtained failure shear values no clear conclusions can be made on which technique is the most suitable one. For the shear modulus results obtained with Resonalyser, torsion test and +/-45° tests give values of the same order, while results obtained with 30° off-axis tests and V-notched tests give again values of the same order. However these last values could be too high.

Since only the V-notched tests and +/-45° tests are standard ISO-techniques for the determination of the in-plane shear modulus, preference should be given to these techniques within the Optimat Blades project.